Colloidal Polymers from Dipolar Assembly of Cobalt-Tipped CdSe@CdS Nanorods

Lawrence J. Hill,[†] Nathaniel E. Richey,[†] Younghun Sung,[‡] Philip T. Dirlam,[†] Jared J. Griebel,[†] Eli Lavoie-Higgins,[†] In-Bo Shim,[§] Nicola Pinna,[⊥] Marc-Georg Willinger,[∥] Walter Vogel,[▽] Jason J. Benkoski,[⊗] Kookheon Char,[‡,*] and Jeffrey Pyun[†,‡,*]

[†]Department of Chemistry and Biochemistry, University of Arizona, 1306 East University Boulevard, Tucson, Arizona 85721, United States, [‡]World Class University Program for Chemical Convergence for Energy and Environment, The National Creative Research Initiative Center for Intelligent Hybrids, School of Chemical and Biological Engineering, Seoul National University, Seoul 151-744, Korea, [§]Department of Nano and Electronic Physics, Kookmin University, Seoul, 136-702, Korea, [⊥]Institut für Chemie, Humboldt-Universität zu Berlin, Brook-Taylor-Straße 2, 12489 Berlin, Germany, [∥]Department of Inorganic Chemistry, Fritz Haber Institute of the Max Planck Society, 14195 Berlin, Germany, [▽]Department of Chemistry, National Central University, Jhongli 32001, Taiwan, and [⊗]Milton S. Eisenhower Research Center, The Johns Hopkins University Applied Physics Laboratory, Laurel, Maryland 20723, United States

ABSTRACT The synthesis of a modular colloidal polymer system based on the dipolar assembly of CdSe@CdS nanorods functionalized with a single cobalt nanoparticle "tip" (CoNP-tip) is reported. These heterostructured nanorods spontaneously self-assembled *via* magnetic dipolar associations of the cobalt domains. In these assemblies, CdSe@CdS nanorods were carried as densely grafted side chain groups along the dipolar NP chain to form bottlebrush-type colloidal polymers. Nanorod side chains strongly affected the conformation of individual colloidal polymer bottlebrush chains and the morphology of thin films. Dipolar CoNP-tipped nanorods were then used as "colloidal monomers" to form mesoscopic assemblies reminiscent of traditional copolymers possessing segmented and statistical compositions. Investigation of the phase behavior of colloidal polymer blends revealed the formation of mesoscopic phase separated morphologies from segmented colloidal copolymers. These studies demonstrated the ability to control colloidal polymer composition and morphology in a manner observed for classical polymer systems by synthetic control of heterostructured nanorod structure and harnessing interparticle dipolar associations.

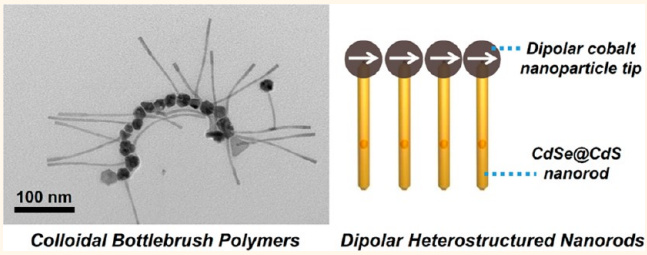

KEYWORDS: colloidal polymers · nanoparticle assembly · dipolar assembly · heterostructured nanorods · ferromagnetic nanoparticles

The use of well-defined inorganic nanocrystals as reagents for the construction of novel colloidal compounds or assemblies is an emerging approach for the preparation of complex mesoscopic materials.[1,2] Controlled large-scale assembly of disparate nanoparticles (NPs) into precisely organized forms is inherently challenging due to thermodynamically driven phase separation of NPs of different size and composition.[3,4] However, a number of recent systems have demonstrated that controlled processing, or precise conjugation of different NPs, enabled the preparation of synergistic hybrid nanocomposites. Seminal work by Murray et al. has demonstrated the concept of using colloidal nanoparticles as "artificial atoms" *via* the coassembly of disparate nanoparticles into nanocrystalline superlattices.[5−7] Similarly, the preparation of "artificial molecules" has been investigated by the chemical conjugation of two or more discrete nanoparticles into heterodimeric nanomaterials.[8−13] A wide variety of synthetic routes to complex heterostructures have been reported that incorporate metal NPs and semiconductor nanorod components for fundamental studies of charge transfer as a function of heterostructure composition and morphology.[14−23]

The use of nanoparticles as "colloidal monomers" for the synthesis of one-dimensional (1-D) mesostructures has received attention toward the formation of "colloidal polymers".[24,25] The seminal work of Kotov et al. demonstrated the polymerization

* Address correspondence to jpyun@email.arizona.edu, khchar@snu.ac.kr.

Received for review August 5, 2013 and accepted March 19, 2014.

Published online March 19, 2014
10.1021/nn406104d

of cadmium telluride (CdTe) quantum dots into extended, continuous CdTe nanowires *via* electrostatic dipolar assembly of colloidal monomers.[26,27] The polymerization of both gold NPs and nanorods (AuNRs) has been reported to form a variety of colloidal (co)polymers.[28−56] Colloidal polymerization of dipolar magnetic nanoparticles has also been extensively investigated using ferromagnetic metal colloids (e.g., Fe, Co, Ni) where the magnetic spin dipole intrinsically embedded in certain ferromagnetic dipolar NPs allowed for strong, directional associations to form colloidal polymers.[57−76] We have previously studied the synthesis and assembly of dipolar CoNPs and core@shell Au@CoNPs to form magnetic colloidal polymers and cobalt oxide nanomaterials.[76] Similarly, reports by numerous groups, notably Gast, Bibette, and Pine et al., have demonstrated the formation of complex microscopic chains *via* assembly of micrometer sized magnetic beads.[77−81] However, the synthesis of complex and multifunctional magnetic dipolar NPs as colloidal monomers has not been as extensively investigated and remains an open avenue for materials chemistry.

While the control of macromolecular structure and architecture has been achieved by controlled and living polymerization methods in classical polymer science,[82] methods to control fundamental structural features, such as chain length, composition, and architecture, are still being developed for NP-based colloidal polymer systems. Applying these "principles of polymerization" to the assembly of NP monomers into colloidal polymers offers a new route to inorganic and nanocomposite materials that cannot be achieved using current nanocrystal synthetic methods.[82] Chen et al. demonstrated that Au colloidal monomers exhibited "unconventional" chain growth features to control both chain length and aggregation motifs of AuNPs into linear chains or clusters of chains.[83] Mechanistic and kinetic studies on the polymerization of AuNR monomers by the tracking of plasmon resonance absorbances enabled precise monitoring of colloidal monomer conversion and fitting of these kinetics to classical step-growth polymerization models.[84−86] A recent example of controlling the degree of polymerization in colloidal polymers was also demonstrated by Kumacheva et al., where heterodimeric Au−Fe_xO_y NPs were used as chain-terminating agents to end-cap growing chains of AuNR colloidal polymers.[87] The application of these new concepts to dipolar magnetic NPs to form colloidal polymers are inherently challenging due to the fast polymerization kinetics of these colloidal monomers and the absence of spectroscopic probes to monitor colloidal monomer conversion.

Herein, we report on the fundamental aspects of the self-assembly and dipolar copolymerization of a novel class of dipolar colloidal monomers with pendant semiconductor nanorods. Heterostructured nanorods based on a cadmium selenide seeded cadmium sulfide (CdSe@CdS) nanorod conjugated to a single dipolar, ferromagnetic cobalt nanoparticle "tip" were chosen due to the synthetic tunability of the semiconductor nanorod inclusion (Scheme 1).[88−94] Seminal work by Banin and Cozzoli elegantly demonstrated the synthesis of CoNP-tipped semiconductor nanorods which were not designed for colloidal polymerization, since nondipolar CoNPs were used as tips for these nanorods.[93,95] By comparison, the colloidal monomers described in this report spontaneously self-assemble into linear colloidal polymer architectures through dipolar coupling of the CoNP-tips. The resulting colloidal polymers are composed of CoNP units in the backbone and CdSe@CdS nanorods carried as side chain groups to form a mesoscopic analogue of a bottlebrush polymer,[96] or "colloidal bottlebrush polymers". Variation of the nanorod length in the CoNP-tipped CdSe@CdS nanorod enabled, for the first time, systematic study of dipolar (co)polymerization processes *via* "grafting through" approaches to form colloidal bottlebrush polymers. By either blending of disparate colloidal monomers or *in situ* deposition of dipolar CoNP-tips onto nanorods of varying length, homopolymers, segmented block-type, and statistical copolymer compositions were obtained. Furthermore, due to the strong dipolar associations between dipolar CoNPs in colloidal polymers, the phase behavior of blends of "bare" CoNP colloidal polymers with CoNP-tipped nanorod colloidal bottlebrush polymers demonstrated that these mesoscopic polymers exhibited phase behavior reminiscent of classical polymer systems.

Scheme 1. Synthesis of dipolar colloidal monomers from heterostructured nanorods.[a]

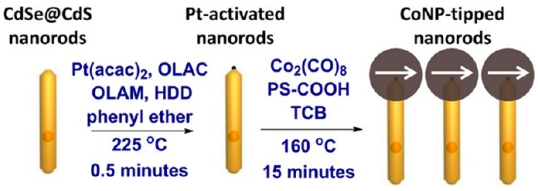

[a] CdSe@CdS nanorods were modified by a brief Pt-activation reaction which preferentially activated these nanorods towards cobalt deposition at the sulfur-rich nanorod terminus with minimal deposition of Pt onto the nanorod. Dipolar CoNP-tips were then deposited onto these activated CdSe@CdS nanorods at primarily one terminus per nanorod (matchstick morphology), and the CoNP-tips spontaneously assembled into chains due to magnetic interactions. Abbreviations: OLAC = oleic acid; OLAM = oleylamine; HDD = 1,2-hexadecanediol; PS-COOH = carboxylic acid terminated polystyrene[65] (M_n = 8600 g/mol; PDI = 1.07); TCB = 1,2,4-trichlorobenzene. Ligands are omitted for clarity.

RESULTS AND DISCUSSION

Preparation of Dipolar CoNP-Tipped CdSe@CdS Nanorods. Dipolar cobalt-tipped CdSe@CdS nanorods were

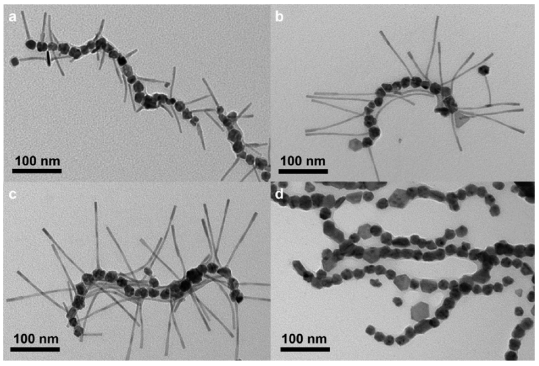

Figure 1. TEM images: (a) CoNP-tipped CdSe@CdS nanorods ($L_{nanorod}$ = 66.0 ± 5.5 nm, $D_{nanorod}$ = 5.3 ± 0.6 nm; $D_{CoNP\text{-}tip}$ = 20 ± 4 nm); (b) CoNP-tipped CdSe@CdS nanorods ($L_{nanorod}$ = 124.0 ± 28.2 nm, $D_{nanorod}$ = 5.4 ± 0.7 nm; $D_{CoNP\text{-}tip}$ = 22 ± 3 nm); (c) CoNP-tipped CdSe@CdS nanorods ($L_{nanorod}$ = 150.1 ± 15.9 nm, $D_{nanorod}$ = 5.7 ± 0.9 nm; $D_{CoNP\text{-}tip}$ = 22 ± 4 nm); (d) cobalt nanoparticles (D_{CoNP} = 24 ± 5 nm) synthesized under similar conditions, *without* nanorod seeds. A minimum of 100 particles were analyzed to obtain each size distribution. Scale bars are 100 nm.

synthesized in four steps from commercially available reagents. CdSe quantum dots (diameter (D) = 2.7−3.2 nm) and CdSe@CdS nanorods (length (L) = 53.1−150.1 nm; diameter (D) = 5−6 nm) were synthesized as previously reported[97] on the basis of the work of Manna et al.[98] In the key step of the synthesis, the Pt-deposition conditions reported by Mokari and coworkers[99] to activate CdSe@CdS nanorods were modified to enhance specificity for deposition of a single, dipolar CoNP-tip ($D_{CoNP\text{-}tip}$ = 24 nm ± 5 nm, Scheme 1).[97] A series of "matchstick" dipolar CoNP-tipped nanorods were then prepared with systematic variation of CdSe@CdS nanorod length using our established conditions to grow ferromagnetic CoNPs (Figure 1).[63,65,69] Using this synthetic method, Pt-activated CdSe@CdS nanorods were tipped with a single ferromagnetic CoNP with a small percentage (10 mol %) of free CoNPs (without nanorods) formed in the reaction. Synthetic procedures and characterization of these materials are provided in the Supporting Information.

Colloidal Polymers from Dipolar CoNP-Tipped CdSe@CdS Nanorods. Heterostructured nanorods composed of dipolar CoNP-tips deposited onto Pt-activated CdSe@CdS nanorods were sufficiently dipolar at room temperature and zero-field conditions to spontaneously form linear assemblies. These CoNP-tipped nanorods were analogous to macromonomers that when homopolymerized *via* "grafting through" methods formed bottlebrush polymers,[96] where dipolar association of CoNP-tips formed the colloidal polymer backbone. These self-assembled colloidal polymers were composed of CoNP chains that carried semiconductor nanorods as side chain groups in nearly every repeating unit of the dipolar NP chain. Nanorod side chains were frequently observed to adopt extended conformations relative to the CoNP-tip (colloidal polymer) backbone in a manner visually reminiscent of AFM studies of bottlebrush polymers[96] where the CdSe@CdS nanorod was often observed to be oriented perpendicular to the magnetic dipole of the CoNP-tip. The selective 1-D assembly of these heterostructured colloids indicated that CdSe@CdS nanorods were solely oriented perpendicular to the CoNP magnetic dipole. This is an important structural feature of these colloidal monomers because it allowed repetitive connectivity of the "polymerizable" magnetic moieties (CoNP-tips) and minimized steric hindrance from the nanorod side chains during the assembly process. If the attached nanorods were not perpendicular to the CoNP magnetic dipole, then the formation of dipolar dimers, or small clusters, would likely have resulted due to steric screening of either the north or south dipole of the CoNP with the nanorod side chain. While the causality of the nanorod perpendicular orientation relative to the CoNP dipole is pending further investigation, the Pt-activation of CdSe@CdS nanorods likely deposited very small Pt-tips that directed the growth (and easy axis) of the resulting CoNP-tip. TEM further revealed that nanorod side chains were commonly found to adhere to, or associate along, the CoNP-tip backbone and associate with other nanorod side chains, which resulted in significant bending of nanorods when cast onto a supporting substrate (Figure 1b,c). The formation of conformations with "bent" side chains was more pronounced in dipolar assemblies formed with longer nanorods having larger aspect ratios (Figure 1). Similar bending of Au nanowires, carbon nanotubes, MnO_2 nanowires, and Pd nanowires by polymeric nanoconfinement and tension at oil/water interfaces was observed previously by Chen et al.[100−102]

To further investigate the effects of nanorod side chain groups on the gross morphology of dipolar colloidal polymer chains, thicker, entangled films of dipolar chains were cast and imaged on carbon-coated TEM grids (Figure 2). Bare dipolar CoNPs along with heterostructured nanorods possessing dipolar CoNP-tips of comparable particle size were selected for these studies, where the only structural differences were the presence of CdSe@CdS nanorod side chains of varying length (Figure 2). In concentrated regions of these samples, colloidal polymers from bare dipolar CoNPs were observed to form bundles up to several micrometers in width (Figure 2a,d). Colloidal polymers from CoNP-tipped nanorods with short nanorod side chains (L = 53 nm) also formed bundled networks of chains; however, the degree of lateral aggregation was considerably mitigated by the presence of nanorod side chains (Figure 2b,e). Strikingly, large-scale lateral aggregation was almost completely suppressed for CoNP-tipped nanorods with longer nanorod side chains (L = 150 nm). These chains exhibited minimal aggregation of colloidal polymer chains as a direct consequence of the steric isolation of CoNP colloidal

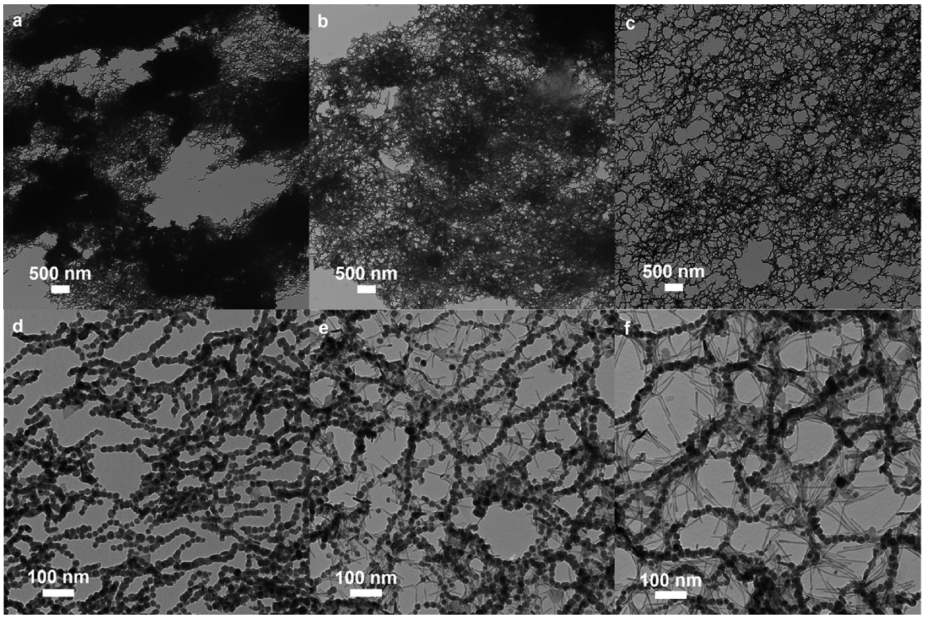

Figure 2. TEM images: (a,d) CoNPs without attached nanorods (D_{CoNP} = 21 nm); (b, e) "short" CoNP-tipped nanorods ($D_{CoNP\text{-}tip}$ = 22 nm; $L_{nanorod}$ = 53 nm); (c, f) "long" CoNP-tipped nanorods ($D_{CoNP\text{-}tip}$ = 22 nm; $L_{nanorod}$ = 150 nm). TEM samples were dried in an external magnetic field to induce lateral bundling of NP chains. Scale bars are 500 nm for the top row of images and 100 nm for the bottom row of images.

polymer backbones from longer nanorod side chains (Figure 2c,f). Overall, these findings were in agreement with the previous findings of Hatton et al., where lateral association of dipolar colloidal chains from bare CoNPs was observed due to out of registry association of north−south magnetic dipoles from neighboring particle units.[103] However, colloidal bottlebrush polymers, particularly with increasing nanorod side chain length, suppressed lateral bundling of CoNP polymer backbones due to enhanced steric screening from nanorod side chain groups. The enhanced steric screening of CoNP polymer backbones with longer nanorod side chains were in good agreement with improved site isolation of polymer backbones in poly(methyl methacrylate) molecular bottlebrush polymers as observed by Sheiko and Matyjaszewski et al., with increasing lengths of grafted side chains.[104]

FE-SEM was conducted to image individual colloidal bottlebrush polymers cast onto carbon coated TEM grids as a function of different nanorod side chain lengths (Figure 3). FE-SEM imaging at high tilt angle revealed that CdSe@CdS nanorods were preferentially oriented perpendicular to the CoNP backbone, where these nanorod side chains tended to spread onto the carbon surface (Figure 3). As observed in TEM, longer nanorod side chains (L = 124 nm) on colloidal polymers were more commonly observed to be bent when compared to shorter nanorods (L = 53 nm) with similar diameters (5.4 nm). More strikingly, FE-SEM of colloidal polymers assembled from CoNP-tipped nanorods with longer side chains indicated more efficient wetting on the carbon-coated substrate as noted by spreading of CdSe@CdS nanorods, affording flattened wormlike

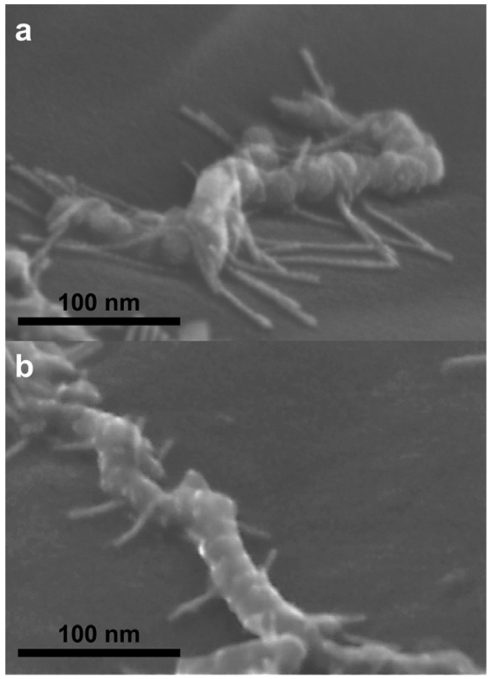

Figure 3. FE-SEM images: (a) CoNP-tipped nanorods with long nanorod side chains ($L_{nanorod}$ = 124 nm, $D_{nanorod}$ = 5.4 nm; $D_{CoNP\text{-}tip}$ = 22 nm); (b) CoNP-tipped nanorods with short nanorod side chains ($L_{nanorod}$ = 53 nm, $D_{nanorod}$ = 5.4 nm; $D_{CoNP\text{-}tip}$ = 22 nm). Scale bars are 100 nm. Samples for FE-SEM imaging were cast onto carbon-coated TEM grids and mounted at 90° relative to the incident beam.

assemblies (Figure, 3a). Similar polymeric nanostructures have been observed by Matyjaszewski and Sheiko et al., with bottlebrush polymers, where poly(*n*-butyl acrylate) side chains were imaged using AFM.[96] The presence of both long nanorods and hydrophobic

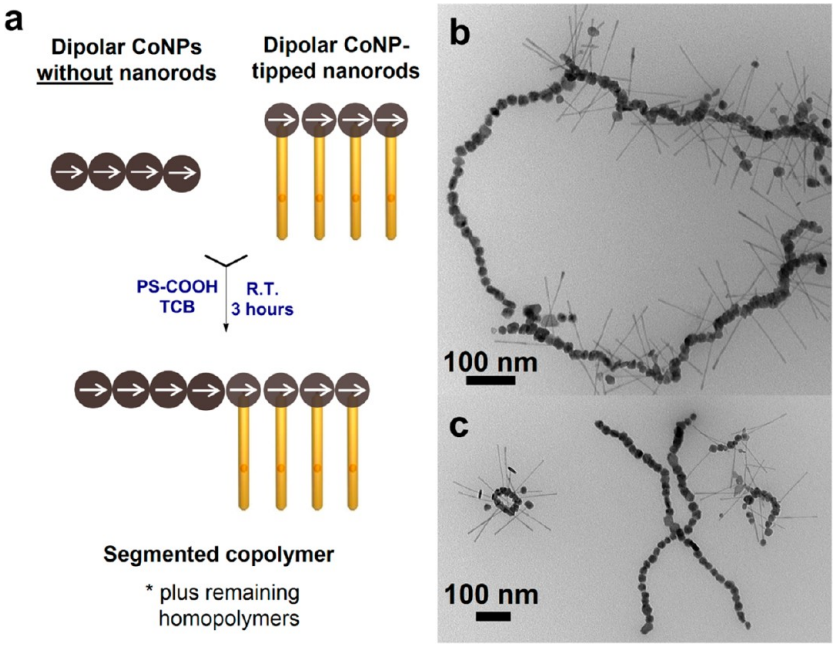

Figure 4. (a) Synthetic scheme for blends of dipolar bare CoNPs and CoNP-tipped nanorods to form segmented colloidal copolymers. (b) TEM image of CoNP-tipped nanorods ($L_{nanorod}$ = 124 nm; $D_{CoNP\text{-}tip}$ = 22 nm) blended with free CoNPs (D_{CoNP} = 24 nm) in solution for 3 h at room temperature (1:1 molar ratio; ca. 6 × 10^{-9} M nanoparticles, Supporting Information). (c) TEM image of residual nonconjugated "homopolymer" chains also present after blending dipolar colloids. Scale bars are 100 nm.

aliphatic small molecule ligands on the nanorods likely promoted this spreading onto the substrate.

Conversely, FE-SEM of colloidal polymers assembled with shorter nanorod side chains exhibited more diverse chain conformations due to positioning of side chain nanorods around the colloidal polymer backbone. While these shorter nanorods were periodically observed to spread onto carbon coated grids as in the case of longer nanorods, these short nanorods were also observed to "prop up" segments of the CoNP chains due to end-on vertical orientation of nanorods on the supporting substrate (Figure 3b). Furthermore, relative to colloidal polymers containing longer nanorod side chains, FE-SEM imaging of colloidal polymers with shorter nanorods suggested a decrease in the apparent density of nanorod side chains, since not all of the shorter nanorods were observed to spread on the supporting substrate. However, TEM of these assemblies (Figure 1) confirmed that presence of a very high yield of CoNP-tipped nanorods (~90%), which indicated that a fraction of these shorter nanorods were hidden by the CoNP backbone at the high tilt angle imposed for FE-SEM imaging. Although nanorod side chains affected colloidal polymer chain conformation, TEM and FE-SEM imaging of dipolar CoNP-tipped nanorods demonstrated that dipolar associations dominated the assembly of these colloids into 1-D chains (Figure 1, Figure 3, and Figure S-5 (Supporting Information)).

Co-assembly Experiments with Dipolar Nanoparticles and Dipolar CoNP-Tipped Nanorods. With a family of dipolar CoNP-tipped nanorods and CoNPs in hand, the coassembly of disparate dipolar colloids into mesoscopic NP chains was investigated as a route to vary the composition in colloidal polymer chains. CoNPs with diameters and magnetic properties similar to those currently studied were previously observed to exist as tightly associated chains of NPs in the dispersed state.[66,67] From the perspective of using these dipolar colloids to form "colloidal *co*polymers," a key question to examine was whether disparate dipolar nanoparticles preferred to self-associate into their own NP chains or coassemble into NP chains with random sequencing of the disparate NP units.

In this series of coassembly experiments, CoNP-tipped nanorods were blended in an equimolar ratio with free CoNPs possessing similar size and magnetization (Figure 4). TEM imaging under zero-field conditions indicated the formation of segmented NP chains composed of CoNP units linked to CoNP-tipped nanorods units, resembling block copolymers (Figure 4a,b). Concurrently, "homopolymer" chains of nonconjugated CoNPs and CoNP-tipped nanorods were also observed (Figure 4c). Statistics taken from TEM images (n > 1000) showed that approximately 77% of CoNPs and CoNP-tipped nanorods were incorporated into "segmented copolymer" assemblies (Table S3, see the Supporting Information).

Co-assembly experiments were also conducted by blending preformed dipolar CoNP-tipped nanorods of differing lengths to exclude any differences in the magnetic properties of free CoNPs and CoNP-tipped nanorods that would affect coassembly (Figure 5). Nanorod side-chain length was a useful probe for visualizing the composition of these segmented

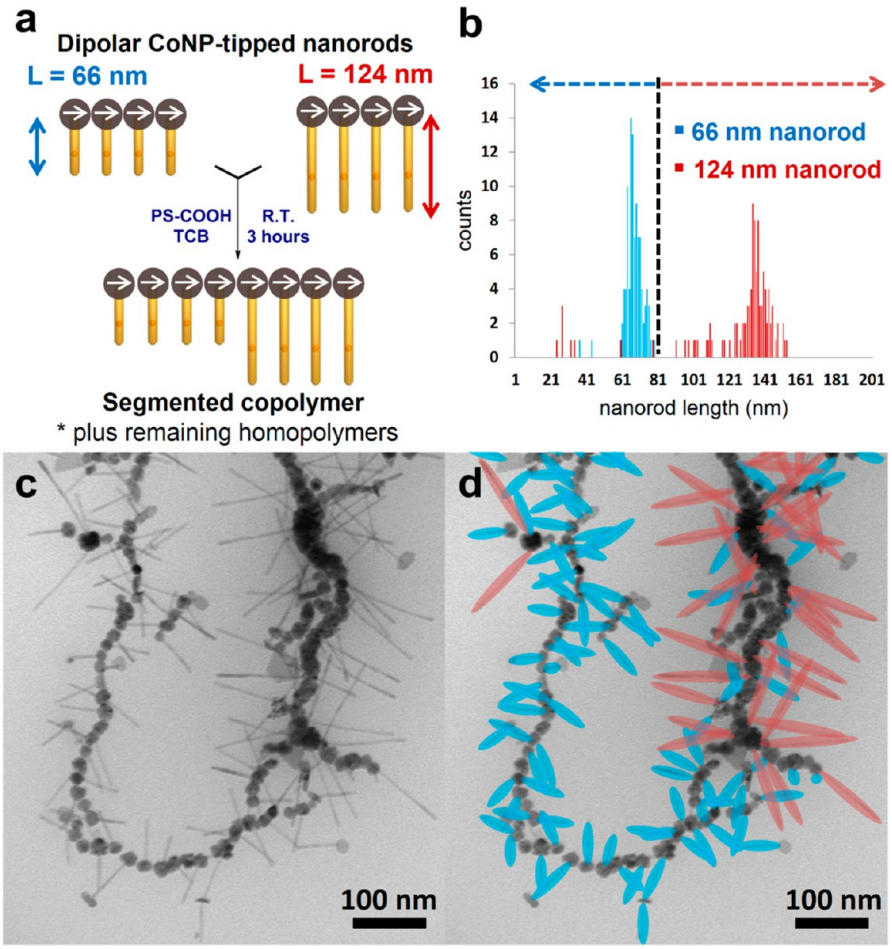

Figure 5. (a) Synthetic scheme for blends of dipolar CoNP-tipped nanorods having two nanorod lengths (L_1 = 66 nm and L_2 = 124 nm) to form segmented colloidal copolymers. Nanorods were blended in a 1:1 molar ratio (ca. 2 × 10^{-9} M nanoparticles). (b) Histogram showing nanorod length distributions prior to cobalt deposition, where the 66 nm nanorods are colored blue and the 124 nm nanorods are colored red. (c) TEM image of a segmented copolymer chain. (d) False colored TEM image from (c). Nanorod side chains in the TEM image were colored red if their measured length was >80 nm, while all other nanorod side chains were colored blue. Scale bars are 100 nm.

colloidal copolymers consisting of dipolar CoNP-tipped nanorods, where the length distributions obtained for the parent nanorods were sufficiently different to enable image analysis and color contrasting of longer vs shorter nanorods (Figure 5b,d). TEM imaging of these assemblies indicated the formation of segmented NP chains composed of CoNP-tipped nanorod segments of different lengths segregating into their own 1-D domains resembling block, or segmented, copolymers as described in the previous blending experiment. The phenomenological conclusions were also consistent with blending experiments with preformed dipolar CoNP-tipped nanorods and CoNPs shown in Figure 4 which formed both homopolymer and segmented copolymer NP chains. Statistics taken from TEM images (n > 1000) showed that approximately 72% of CoNP-tips were incorporated into "segmented copolymer" assemblies (Table S4, Supporting Information).

Mechanism for the Formation of "Segmented Copolymers". The formation of "segmented copolymer" mesostructures and the persistence of residual "homopolymers" pointed to the persistence of short chains of dipolar nanoparticles in a kinetically frozen state during mixing (nonergodic mixing).[66,67] Dipolar NPs existed primarily as dipolar assemblies (as opposed to individually dispersed NPs) due to the large energetic gain for dipolar coupling between dipolar colloids. This energy can be calculated using eq 1, where μ is the dipole moment of the nanoparticle, μ_r is the relative permeability of water, μ_0 is the permeability of free space, and r is center to center distance of nanoparticles in contact.[105,106] To a first approximation, CoNPs with a 22 nm diameter, 3 nm thick PS corona, and 76.8 emu/g magnetization possess an association energy of $-32k_BT$ on contact, which greatly exceeds thermal energy and strongly favors the assembled state of NP chains. This large association energy dictates that vanishingly small amounts of nanoparticles will be individually dispersed at any given time (about one in 10^{14} particles).[105,106]

$$E = -\frac{\mu^2}{2\pi\mu_r\mu_0 r^3} \quad (1)$$

Scheme 2. Proposed mechanism for formation of "block copolymers".[a]

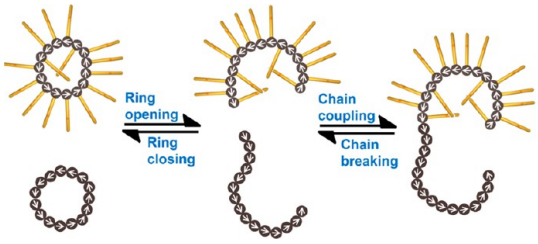

[a] White arrows represent magnetic dipoles present in CoNPs and CoNP-tips.

Simulations of equilibrium polymerization in a Stockmayer fluid reproduce many experimental observations of magnetic nanoparticle self-assembly,[105,106] where Stockmayer fluids that undergo equilibrium polymerization exist as loops, linear chains, and hybrid branched structures all in dynamic equilibria.[107−111] Therefore, the postulated mechanism for block formation in mixtures of CoNPs with CoNP-tipped nanorods dealt with the interactions of these assemblies (Scheme 2). Prior to mixing, individual CoNP- and CoNP-tipped nanorod suspensions consisted primarily of homopolymer chains, loops, and branched structures (not shown) formed during synthesis or shortly thereafter. When the two suspensions were blended together, one initially obtained a mixture of homopolymers, and copolymerization could only occur when the north pole of one chain end coupled to the south pole of another (i.e., loops can only copolymerize when they open temporarily due to thermal fluctuations).[107−111] For the drawing in Scheme 2 to be true, the dipolar interactions must be in a regime where the equilibrium strongly favors the assembled NP chain state prior to mixing but not so strong that the loops are kinetically frozen over experimental time scales. Although the proposed mechanism indicated nothing about the loop-opening kinetics, TEM images such as those in Figure 4 clearly demonstrated the availability of chain ends for forming segmented copolymers. This mechanism also applied to blends of dipolar CoNP-tipped nanorods (Figure 5).

In order for "random" or "statistical copolymers" of CoNPs and CoNP-tipped nanorods to form, dipolar nanoparticles would have to be mixed as individually dispersed nanoparticles prior to assembly. The complete absence of statistical copolymers therefore meant that individually dispersed CoNPs were present in vanishingly small concentrations throughout the experiment due to predominant association of NPs into colloidal chains. Therefore, additional blending experiments were conducted to determine if randomization of dipolar colloids could be achieved to promote formation of "statistical colloidal copolymers" by strong sonication of dispersion, application of alternating magnetic field, or dilution and heating of the dispersed blends (Figures S-8 and S-9, Supporting Information). However, in all of these experiments, randomization of disparate dipolar colloids was not observed, supporting our hypothesis that dipolar colloids tended to reside as short NP chains when dispersed in solution.

Additional chemical evidence was collected to support this proposed mechanism *via* acid etching of strongly dipolar CoNP-tipped nanorods.[112] Chemical etching of metallic cobalt phases using oleic acid was found sufficient to reduce CoNP-tip diameters (from $D = 22 \pm 4$ nm to $D = 17 \pm 4$ nm) and weakened interparticle magnetic associations. Contrary to previous blending studies (as shown in Figures 4 and 5), the formation of randomized coassemblies were observed by TEM which supported our proposed mechanism where strong dipolar interactions prevented random incorporation of individual colloidal monomers into colloidal copolymer chains (Figure S-10, Supporting Information).

Statistical Colloidal Copolymers from Blending Pt-Activated Nanorods Prior to Cobalt Deposition. As previously discussed, blends of disparate dipolar colloids afforded mixtures of both segmented and homopolymer chains due to nonergodic mixing of the individual magnetic nanoparticles. Furthermore, despite attempts to induce isotropic dispersion and mixing of disparate dipolar colloids, the strong dipolar associations holding NP chains together dominated the coassembly and suppressed the formation of statistical colloidal copolymers with random sequencing of nanorods along the copolymer backbone.

A chemical solution to this problem was to blend dispersions of Pt-activated CdSe@CdS nanorods of different lengths and then deposit CoNP-tips to form *in situ* mixtures of dipolar nanorods. This chemical approach ensured isotropic mixing of nanorods of varying size and was more true to a "grafting through" approach, since these precursors did not self-associate prior to deposition of ferromagnetic CoNP-tips. Using this method, dipolar CoNP-tipped CdSe@CdS nanorods were prepared which afforded CoNP-tips on both lengths of nanorods simultaneously (Figure 6). These CoNP-tips were similar in size and morphology to those observed for cobalt deposition onto a single nanorod length (e.g., Figure 1). Unlike the previous coassembly experiments with preformed dipolar colloids, these dipolar assemblies exclusively formed random copolymer-like NP chains as imaged by TEM. Furthermore, the presence of homopolymer chains composed of nanorods of similar length was *not* observed as a consequence of this *in situ* Co-deposition methodology. The ability to prepare random copolymer assemblies *via* this chemical methodology further confirmed that random copolymer sequences were accessible *via* coassembly of disparate dipolar colloids, but blending conditions to achieve isotropic mixing are complicated by the inherently strong magnetic associations

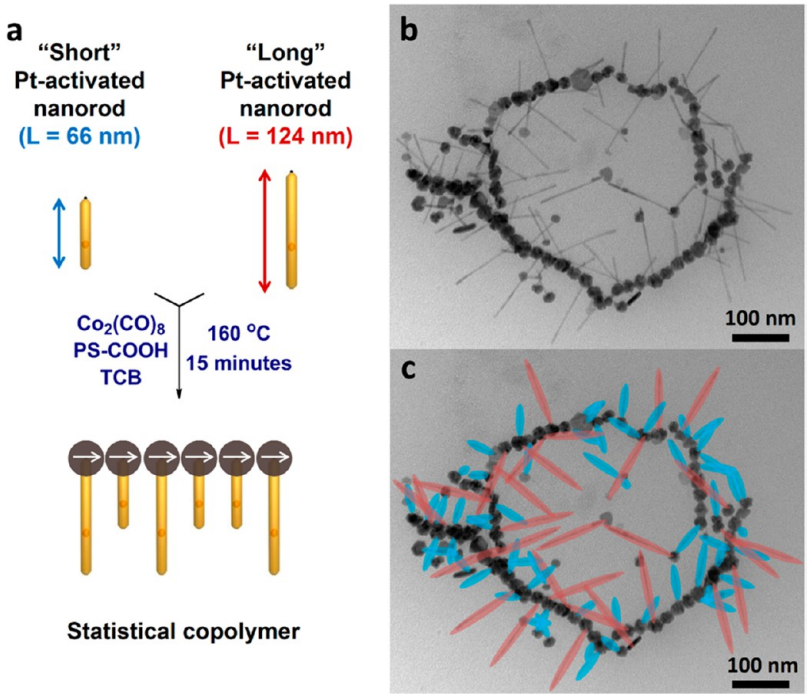

Figure 6. (a) Synthetic scheme for synthesis of statistical colloidal copolymers by deposition of CoNP-tips onto a 1:1 mixture of differing lengths of Pt-activated nanorods (L_1 = 66 nm and L_2 = 124 nm). (b) TEM image of a statistical copolymer chain after cobalt deposition (CoNP-tip diameter = 22 nm ±4 nm). (c) False colored TEM image from Figure 6b. Color labels were chosen based on nanorod length distributions as described in the caption for Figure 5, and "homopolymers" were *not* observed. Scale bars are 100 nm.

of the ferromagnetic CoNPs and CoNP-tips used in this study.

Phase Behavior of Colloidal Copolymers. Finally, the phase behavior of segmented colloidal copolymer chains was investigated to ascertain if nanorod side chains would induce phase separation when blended with colloidal polymers from bare CoNPs (Figure 7). Mesoscopic chains were anticipated to retain their connectivity due to the strong coupling between CoNPs and CoNP-tips in colloidal polymers, as discussed above for segmented colloidal copolymers. This would enable for the first time interrogation of the phase behavior of mesoscopic colloidal polymers to observe if phenomenon such as mixing versus phase separation would occur. In our investigations of segmented copolymers, dipolar chains were observed to phase separate into regions enriched in segments of bare CoNPs or CoNP-tipped nanorods. Under these conditions, colloidal polymers containing nanorod side chains were observed to form a semicontinuous matrix phase due to their larger occupied area per nanoparticle, while bare CoNP chains phase segregated into more densely bundled domains.

To amplify this effect, a segmented colloidal copolymer sample was prepared from CoNPs and CoNP-tipped nanorods as in Figure 4 above, with a 10-fold molar excess of CoNPs. In these blended samples, the formation of microscopic domains reminiscient of a phase separated spherical morphology in block copolymer thin films were observed in the formation of tightly bundled domains of bare CoNP chains spaced with a quasicontinuous phase of nanorod-bearing colloidal polymers (Figure 7). However, it is important to note that these more ordered regions were also accompanied by presence of larger, less ordered, phase-separated regions of colloidal polymers of bare CoNPs (Figure S-13, Supporting Information). Nevertheless, these blending experiments demonstrate that

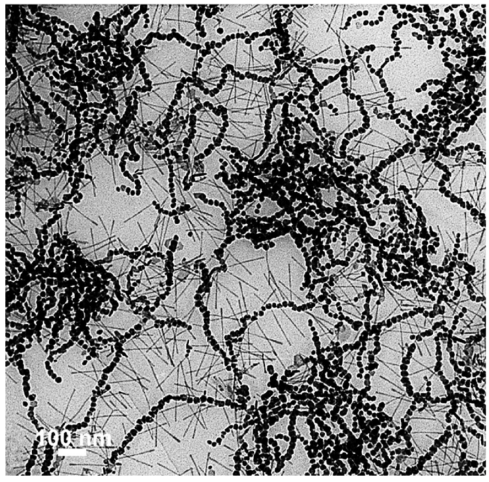

Figure 7. TEM image of CoNPs (D = 21 nm; without nanorod side chains) and CoNP-tipped nanorods ($D_{CoNP\text{-}tip}$ = 22 nm; $L_{nanorod}$ = 150 nm) blended in a 10:1 molar ratio. Scale bar is 100 nm. TEM samples were prepared under zero field conditions.

dipolar colloidal (co)polymer chains exhibit striking phase behavior similar to conventional (co)polymer systems.

CONCLUSIONS

In conclusion, we have demonstrated the self-assembly of dipolar CoNP-tipped CdSe@CdS nanorods into colloidal bottlebrush polymers. These colloidal polymers are composed of a CoNP backbone with a high grafting density of CdSe@CdS nanorod side chains which strongly influence the conformation and morphology of the colloidal polymer chains. Strong magnetic interactions of these dipolar CoNP-tips enabled the formation of magnetic colloidal copolymers with segmented compositions for the first time. Our modular synthesis approach was utilized as a means of overcoming the tendency for the formation of blocky structures, where blending nondipolar precursors allowed the formation of randomly connected colloidal monomers within the polymeric mesostructures (statistical copolymers). This system is one of the few examples where colloidal polymers and copolymers of different composition can be controlled on the mesoscale. Finally, the phase behavior of these colloidal polymers was investigated to demonstrate that microphase separation concepts from traditional polymer science are applicable to colloidal polymers.

METHODS

Materials and Characterization. 1,2,4-Trichlorobenzene (TCB) (>99%) was purchased from both Aldrich and Alfa Aesar and passed through a 0.2 μm syringe filter prior to use. 1,2-Dichlorobenzene (DCB) (>99%) was purchased from both Aldrich and Acros Organics and passed through a 0.2 μm syringe filter prior to use. 1,2-Hexadecanediol (HDD) (90%), toluene (99.5%), cadmium(II) oxide (CdO) (99.5%), selenium (99.999%), oleic acid (OLAC) (90%), oleylamine (OLAM) (70%), and 1-octadecene (ODE) (90%) were purchased from Aldrich. Octadecylphosphonic acid (ODPA) (97%), trioctylphosphine oxide (TOPO) (99%), trioctylphosphine (TOP) (90%), trioctylphosphine (TOP) (97%), hexylphosphonic acid (HPA) (97%), and dicobalt octacarbonyl stabilized with 5% hexanes ($Co_2(CO)_8$) were purchased from Strem. Platinum(II) acetylacetonate ($Pt(acac)_2$) (98%) and diphenyl ether (DPE) (99%) were purchased from Acros Organics. Sulfur (>99.0%) was purchased from EMD, and absolute ethanol (EtOH) was purchased from Pharmco-Aaper. All chemicals were commercially available and used as received, unless otherwise noted. Air-free manipulations were performed under argon by using standard Schlenk techniques with vacuum pressure at approximately 1 mmHg using an Edwards High Vacuum International vacuum pump (Model RV12, Sussex England). An Omega temperature controller CSC32K with a K-type utility thermocouple and a Glas-Col fabric heating mantle were used for thermolysis reactions. All centrifugation steps were performed in 50 mL centrifuge tubes using a rotor with a radius of 11 cm. UV−vis measurements were obtained using a Shimadzu Corp. UV−vis recording spectrophotometer (no. UV-2401PC, Kyoto Japan). Fluorescence measurements were obtained using a Photon Technology International spectrometer (no. 3005, Weatherford TX). Low resolution bright field TEM images (those *not* labeled "high resolution") were obtained on a Phillips CM12 transmission electron microscope (CM12) at 80 kV, or a Tecai Spirit transmission electron microscope (FEI) at 100 kV using in house prepared carbon coated copper grids (Cu, hexagon, 200 mesh). Image analysis was performed using ImageJ software (Rasband, W.S., National Institutes of Health, http://rsb.info.nih.gov/ij/, 1997−2007) from bright field TEM images at a minimum of 110000× magnification by sizing a minimum of 100 particles (unless otherwise stated). Relative uncertainty of particle size determinations using ImageJ was found to be 1% of diameter average (e.g., 20 ± 0.2 nm). High-resolution TEM (HRTEM) images were obtained using a CM200FEG (Philips) microscope with a field emission gun operated at 200 kV. Thermogravimetric analysis was carried out under nitrogen atmosphere using a TGA Q50 instrument and software from TA Instruments. VSM measurements were conducted using a Waker HF 9H electromagnet with a Lakeshore 7300 controller and a Lakeshore 668 power supply. Magnetic measurements were carried out at room temperature (27 °C or 300 K) with a maximum S-2 applied field of 1190 kA/m, a ramp rate of 2630 Am-1s-1 and a time constant of 0.1. XRD measurements were performed on the μSpot beamline at BESSY II synchrotron. A Si 111 Monochromator was used and an incident X-ray energy of 12.48 keV (0.9933 Å) was selected. The beam size was 100 μm. A polymer sample holder with 2 mm holes and a thickness of about 1 mm was used. Samples were filled into the holes and covered with Scotch tape. To protect the area detector (MAR-CCD), the primary beam was blocked by a 3.5 mm beam stop made of lead. Each sample was measured twice with an acquisition time of 150 s. The program Fit2D was used for integration of the images. XPS characterization was performed on a KRATOS 165 Ultra photoelectron spectrometer, using a monochromatic Al Kα radiation source. SEM images were taken on a Hitachi 4800 FE-SEM (30 kV accelerating voltage) on the as-prepared sample (*i.e.*, no metallic overcoating).

Note: Full synthetic details for all of the materials described in this report are provided in the Supporting Information; however, representative procedures for the synthesis of Pt-activated CdSe@CdS nanorods and Co-tipped CdSe@CdS nanorods are discussed below.

Representative Procedure for the Synthesis of Pt-Activated CdSe@CdS Nanorods (CdSe Seed: D = 2.7 nm; nanorod: L = 69.1 nm, D = 6.0 nm). CdSe@CdS nanorods (approximately 40 nanomol, 270 mg for 69.1 nm × 6.0 nm nanorods with 17.7% organic content by mass) were weighed into a 20 mL vial and dispersed in 1,2-dichlorobenzene (6 mL) *via* vortex agitation, where sonication in certain cases was briefly applied (<2 min). A solution of platinum(II) acetylacetonate (5 mg in 0.5 mL DCB; 12.7 μmol) was then injected into the vial containing the nanorod dispersion no more than 5 min prior to use. Diphenyl ether (50 mL at 40 °C), oleic acid (1.0 mL; 3.05 mmol), oleylamine (1.0 mL; 3.15 mmol), and 1,2-hexadecanediol (215 mg; 0.85 mmol) were weighed into a 100 mL three-neck-round-bottom flask equipped with a reflux condenser and 1 in. magnetic stir bar. The flask was fitted with rubber septa, and a temperature probe was passed through a septum until it came into direct contact with the solution. The solution was then heated to 80 °C *in vacuo* for 30 min using a heating mantle and temperature controller with continuous stirring at 300 rpm and subsequently backfilled with Ar. The contents of the flask were then heated to 225 °C under argon, followed by injection *via* syringe of CdSe@CdS nanorods dispersed in a solution of $Pt(acac)_2$/DCB (described above) to the reaction mixture. The heating mantle was removed from the reaction flask after 30 s from the injection of $Pt(acac)_2$/nanorods/DCB. Toluene (20 mL) was injected *via* syringe into reaction mixture once the internal temperature of the medium reached 100 °C, and the orange dispersion was allowed to cool to room temperature prior to purification. Purification of as synthesized Pt-activated nanorods in this toluene dispersion was accomplished *via* three cycles of dissolution, precipitation, and centrifugation. The room temperature, crude product

(*i.e.*, toluene dispersion) was divided evenly between four centrifuge tubes, and the contents of each tube were diluted with toluene (to 30 mL) before dilution with EtOH (15 mL) to induce precipitation. Centrifugation of this heterogeneous mixture (3500 rpm, 12 min) afforded orange pellets. The clear supernatants were decanted, and the pellets were each dispersed in toluene (30 mL) before each was diluted with EtOH (15 mL). Centrifugation (3500 rpm, 12 min) a second time afforded orange pellets. The yellow-tinted, translucent supernatants from the various tubes were decanted, and the pellets were each dispersed in toluene (30 mL) before each was diluted with EtOH (15 mL). Centrifugation (3500 rpm, 12 min) a third time resulted in orange pellets. The yellow-tinted, translucent supernatants were decanted, and the resulting precipitate was dispersed in DCM (approximately 10 mL) before a sample was taken for TEM in toluene (DCM dispersion (0.2 mL) diluted into toluene (3 mL) in a separate vial). The DCM dispersion was transferred into a tared vial *via* glass pipet, and the solvent was evaporated before drying the sample *in vacuo* at 55 °C overnight to yield an orange powder (202 mg, 14.9 wt % organic content by TGA).

Representative Procedure for the Synthesis of Dipolar CoNP-Tipped CdSe@CdS Nanorods (Nanorod: L = 124.0 nm, D = 5.4 nm). Pt-activated CdSe@CdS nanorods (9.2 mg, approximately 0.73 nanomol) were loaded into a 20 mL vial containing PS-COOH (10 mg; 1.2 μmol), and TCB (1 mL) was added before the vial was fitted with a screw top polypropylene cap and subjected to 10 min sonication. A 10 mm magnetic stir bar was added to the vial after sonication, and the vial was fitted with a rubber septum. A temperature probe was passed through the septum until it came into direct contact with the reaction mixture before securing the septum with electrical tape. The reaction vessel was evacuated for 2 min and backfilled with argon before heating to 160 °C using a heating mantle and temperature controller with continuous stirring (1000 rpm). Upon reaching 160 °C, room-temperature $Co_2(CO)_8$ dissolved in TCB (0.5 mL of the $Co_2(CO)_8$ stock solution described above; approximately 50 mg or 146 μmol of $Co_2(CO)_8$) was injected. The temperature was held at 160 °C for 15 min from the time of injection before the vial was removed from the heating mantle and allowed to cool to room temperature. In the first step of the magnetic purification process, the magnetic stir bar was removed and rinsed using a solution of PS-COOH/TCB (2 mg PS-COOH/mL TCB, 3 mL) to recover the magnetically associated crude product. The recovered mixture was then diluted with DCM (to approximately 12 mL) before being shaken by hand and subjected to vortex agitation, after which the magnetic probe shown in Figure S-2 (see the Supporting Information) was immersed into the dispersion to promote magnetic flocculation of dipolar nanorods onto the exterior of the magnetized assembly. After immersion of the probe into this DCM dispersion for 2 min, a black precipitate was observed to accumulate along the length of the probe. The syringe barrel was detached from the metal cylinder and bar magnet accessory, and the viscous black ink was washed from the sleeve exterior into another vial using PS-COOH/TCB (3 mL). The black dispersion was then diluted to 12 mL with DCM before collecting onto the magnetic probe as above. The entire process was repeated for a total of 3 magnetic collection steps per sample. The pellet obtained from the final magnetic collection step was dispersed in PS-COOH/TCB (3 mL) and a sample was cast directly from this dispersion onto a carbon coated copper grid for TEM imaging (*no* DCM was added to the final product). The product was imaged *via* TEM and sized using ImageJ software (CoNP-tip diameter =22 $\pm$ 3 nm; approximately 83% of dipolar CoNPs imaged carried a nanorod side chain). These CoNP-tipped matchsticks were sensitive to sonication which resulted in an increased number of shorter "broken" free nanorods being observed in sonicated samples. Dipolar CoNP-tipped nanorods were stored as dispersions when intended for further use. Complete drying of samples or sonication of samples resulted in irreversible aggregation and nanorod fracture, respectively.

Conflict of Interest: The authors declare no competing financial interest.

Acknowledgment. This work was funded by the Division of Chemical Science, Geosciences and Biosciences, Office of Basic Energy Sciences of the U.S. Department of Energy (DE-FG03-02ER15753) (L.J.H., J.P.), the NSF (DMR-0645618 for N.E.R., J.P. and DMR-130792 for P.T.D., J.P.), the World Class University Program through the National Research Foundation of Korea funded by the Ministry of Education, Science and Technology (R31-10013) (Y.S.), and the Alfred P. Sloan Foundation (P.T.D., J.P.). K.C. acknowledges financial support from NRF through the National Creative Research Initiative Center for Intelligent Hybrids (2010-0018290). Dr. Ralf Bienert and Dr. Franziska Emmerling from Bundesanstalt für Materialforschung und -prüfung are acknowledged for XRD measurements. Paul Lee from the Laboratory of Electron Spectroscopy and Surface Analysis at the University of Arizona is acknowledged for XPS measurements. Steven Hernandez and the University Spectroscopy and Imaging Facilities (USIF), Tucson, AZ (http://usif.arizona.edu/) are acknowledged for assistance with FE-SEM imaging. Dr. Adam Simmonds is acknowledged for helpful discussions.

Supporting Information Available: Synthetic details and TEM images for control experiments. This material is available free of charge *via* the Internet at http://pubs.acs.org.

REFERENCES AND NOTES

1. Lu, Z.; Yin, Y. Colloidal Nanoparticle Clusters: Functional Materials by Design. *Chem. Soc. Rev.* **2012**, *41*, 6874–6887.
2. Buck, M. R.; Bondi, J. F.; Schaak, R. E. A Total-Synthesis Framework for the Construction of High-Order Colloidal Hybrid Nanoparticles. *Nat. Chem.* **2012**, *4*, 37–44.
3. Dijkstra, M.; van, R. R.; Evans, R. Phase Behavior and Structure of Binary Hard-Sphere Mixtures. *Phys. Rev. Lett.* **1998**, *81*, 2268–2271.
4. Bishop, K. J. M.; Wilmer, C. E.; Soh, S.; Grzybowski, B. A. Nanoscale Forces and Their Uses in Self-Assembly. *Small* **2009**, *5*, 1600–1630.
5. Murray, C. B.; Kagan, C. R.; Bawendi, M. G. Self-Organization of CdSe Nanocrystallites into Three-Dimensional Quantum Dot Superlattices. *Science* **1995**, *270*, 1335–1338.
6. Redl, F. X.; Cho, K. S.; Murray, C. B.; O'Brien, S. Three-Dimensional Binary Superlattices of Magnetic Nanocrystals and Semiconductor Quantum Dots. *Nature* **2003**, *423*, 968–971.
7. Shevchenko, E. V.; Talapin, D. V.; Kotov, N. A.; O'Brien, S.; Murray, C. B. Structural Diversity in Binary Nanoparticle Superlattices. *Nature* **2006**, *439*, 55–59.
8. Gu, H.; Zheng, R.; Zhang, X.; Xu, B. Facile One-Pot Synthesis of Bifunctional Heterodimers of Nanoparticles: A Conjugate of Quantum Dot and Magnetic Nanoparticles. *J. Am. Chem. Soc.* **2004**, *126*, 5664–5665.
9. Teranishi, T.; Inoue, Y.; Nakaya, M.; Oumi, Y.; Sano, T. Nanoacorns: Anisotropically Phase-Segregated CoPd Sulfide Nanoparticles. *J. Am. Chem. Soc.* **2004**, *126*, 9914–9915.
10. Gu, H.; Yang, Z.; Gao, J.; Chang, C. K.; Xu, B. Heterodimers of Nanoparticles: Formation at a Liquid–Liquid Interface and Particle-Specific Surface Modification by Functional Molecules. *J. Am. Chem. Soc.* **2005**, *127*, 34–35.
11. Yanqiu, L.; Qiang, Z.; Nurmikko, A. V.; Shouheng, S. Enhanced Magnetooptical Response in Dumbbell-like Ag-$CoFe_2O_4$ Nanoparticle Pairs. *Nano Lett.* **2005**, *5*, 1689–1692.
12. Yu, H.; Chen, M.; Rice, P. M.; Wang, S. X.; White, R. L.; Sun, S. Dumbbell-like Bifunctional Au–Fe_3O_4 Nanoparticles. *Nano Lett.* **2005**, *5*, 379–382.
13. Choi, S.-H.; Kim, E.-G.; Hyeon, T. One-Pot Synthesis of Copper–Indium Sulfide Nanocrystal Heterostructures with Acorn, Bottle, and Larva Shapes. *J. Am. Chem. Soc.* **2006**, *128*, 2520–2521.
14. Mokari, T.; Rothenberg, E.; Popov, I.; Costi, R.; Banin, U. Selective Growth of Metal Tips onto Semiconductor Quantum Rods and Tetrapods. *Science* **2004**, *304*, 1787–1790.

15. Mokari, T.; Sztrum, C. G.; Salant, A.; Rabani, E.; Banin, U. Formation of Asymmetric One-Sided Metal-Tipped Semiconductor Nanocrystal Dots and Rods. *Nat. Mater.* **2005**, *4*, 855–863.
16. Cozzoli, P. D.; Manna, L. Asymmetric Nanoparticles - Tips on Growing Nanocrystals. *Nat. Mater.* **2005**, *4*, 801–802.
17. Cozzoli, P. D.; Pellegrino, T.; Manna, L. Synthesis, Properties and Perspectives of Hybrid Nanocrystal Structures. *Chem. Soc. Rev.* **2006**, *35*, 1195–1208.
18. Dukovic, G.; Merkle, M. G.; Nelson, J. H.; Hughes, S. M.; Alivisatos, A. P. Photodeposition of Pt on Colloidal CdS and CdSe/CdS Semiconductor Nanostructures. *Adv. Mater.* **2008**, *20*, 4306–4311.
19. Amirav, L.; Alivisatos, A. P. Photocatalytic Hydrogen Production with Tunable Nanorod Heterostructures. *J. Phys. Chem. Lett.* **2010**, *1*, 1051–1054.
20. Costi, R.; Saunders, A. E.; Banin, U. Colloidal Hybrid Nanostructures: A New Type of Functional Materials. *Angew. Chem., Int. Ed.* **2010**, *49*, 4878–4897.
21. Alemseghed, M. G.; Ruberu, T. P. A.; Vela, J. Controlled Fabrication of Colloidal Semiconductor-Metal Hybrid Heterostructures: Site Selective Metal Photo Deposition. *Chem. Mater.* **2011**, *23*, 3571–3579.
22. Buck, M. R.; Schaak, R. E. Emerging Strategies for the Total Synthesis of Inorganic Nanostructures. *Angew. Chem., Int. Ed.* **2013**, *52*, 6154–6178.
23. Banin, U.; Ben-Shahar, Y.; Vinokurov, K. Hybrid Semiconductor-Metal Nanoparticles; From Architecture to Function. *Chem. Mater.* **2013**, *26*, 97–110.
24. Nie, Z.; Petukhova, A.; Kumacheva, E. Properties and Emerging Applications of Self-Assembled Structures Made from Inorganic Nanoparticles. *Nat. Nanotechnol.* **2010**, *5*, 15–25.
25. Pyun, J. Self-Assembly and Colloidal Polymerization of Polymer−Nanoparticle Hybrids into Mesoscopic Chains. *Angew. Chem., Int. Ed.* **2012**, *51*, 12408–12409.
26. Tang, Z. Y.; Kotov, N. A.; Giersig, M. Spontaneous Organization of Single CdTe Nanoparticles into Luminescent Nanowires. *Science* **2002**, *297*, 237–240.
27. Xu, L.; Ma, W.; Wang, L.; Xu, C.; Kuang, H.; Kotov, N. A. Nanoparticle Assemblies: Dimensional Transformation of Nanomaterials and Scalability. *Chem. Soc. Rev.* **2013**, *42*, 3114–3126.
28. Mirkin, C. A.; Letsinger, R. L.; Mucic, R. C.; Storhoff, J. J. A DNA-Based Method for Rationally Assembling Nanoparticles into Macroscopic Materials. *Nature* **1996**, *382*, 607–609.
29. Li, Z.; Chung, S.-W.; Nam, J.-M.; Ginger, D. S.; Mirkin, C. A. Living Templates for the Hierarchical Assembly of Gold Nanoparticles. *Angew. Chem., Int. Ed.* **2003**, *42*, 2306–2309.
30. Caswell, K. K.; Wilson, J. N.; Bunz, U. H. F.; Murphy, C. J. Preferential End-to-End Assembly of Gold Nanorods by Biotin−Streptavidin Connectors. *J. Am. Chem. Soc.* **2003**, *125*, 13914–13915.
31. Park, S.; Lim, J. H.; Chung, S. W.; Mirkin, C. A. Self-Assembly of Mesoscopic Metal-Polymer Amphiphiles. *Science* **2004**, *303*, 348–351.
32. Thomas, K. G.; Barazzouk, S.; Ipe, B. I.; Joseph, S. T. S.; Kamat, P. V. Uniaxial Plasmon Coupling through Longitudinal Self-Assembly of Gold Nanorods. *J. Phys. Chem. B* **2004**, *108*, 13066–13068.
33. Huo, F.; Lytton-Jean, A. K. R.; Mirkin, C. A. Asymmetric Functionalization of Nanoparticles Based on Thermally Addressable DNA Interconnects. *Adv. Mater.* **2006**, *18*, 2304–2306.
34. Xu, X.; Rosi, N. L.; Wang, Y.; Huo, F.; Mirkin, C. A. Asymmetric Functionalization of Gold Nanoparticles with Oligonucleotides. *J. Am. Chem. Soc.* **2006**, *128*, 9286–9287.
35. Zhang, S. Z.; Kou, X. S.; Yang, Z.; Shi, Q. H.; Stucky, G. D.; Sun, L. D.; Wang, J. F.; Yan, C. H. Nanonecklaces Assembled from Gold Rods, Spheres, and Bipyramids. *Chem. Commun.* **2007**, 1816–1818.
36. Nie, Z. H.; Fava, D.; Kumacheva, E.; Zou, S.; Walker, G. C.; Rubinstein, M. Self-Assembly of Metal-Polymer Analogues of Amphiphilic Triblock Copolymers. *Nat. Mater.* **2007**, *6*, 609–614.
37. DeVries, G. A.; Brunnbauer, M.; Hu, Y.; Jackson, A. M.; Long, B.; Neltner, B. T.; Uzun, O.; Wunsch, B. H.; Stellacci, F. Divalent Metal Nanoparticles. *Science* **2007**, *315*, 358–361.
38. Sun, Z. H.; Ni, W. H.; Yang, Z.; Kou, X. S.; Li, L.; Wang, J. F. pH-Controlled Reversible Assembly and Disassembly of Gold Nanorods. *Small* **2008**, *4*, 1287–1292.
39. Wang, X.; Li, G.; Chen, T.; Yang, M.; Zhang, Z.; Wu, T.; Chen, H. Polymer-Encapsulated Gold-Nanoparticle Dimers: Facile Preparation and Catalytical Application in Guided Growth of Dimeric ZnO-Nanowires. *Nano Lett.* **2008**, *8*, 2643–2647.
40. Chen, T.; Yang, M.; Wang, X.; Tan, L. H.; Chen, H. Controlled Assembly of Eccentrically Encapsulated Gold Nanoparticles. *J. Am. Chem. Soc.* **2008**, *130*, 11858–11859.
41. Fava, D.; Nie, Z.; Winnik, M. A.; Kumacheva, E. Evolution of Self-Assembled Structures of Polymer-Terminated Gold Nanorods in Selective Solvents. *Adv. Mater.* **2008**, *20*, 4318–4322.
42. Nie; Fava, D.; Rubinstein, M.; Kumacheva, E. Supramolecular" Assembly of Gold Nanorods End-Terminated with Polymer "Pom-Poms": Effect of Pom-Pom Structure on the Association Modes. *J. Am. Chem. Soc.* **2008**, *130*, 3683–3689.
43. Wang, C.; Xu, C.; Zeng, H.; Sun, S. Recent Progress in Syntheses and Applications of Dumbbell-like Nanoparticles. *Adv. Mater.* **2009**, *21*, 3045–3052.
44. Tan, L. H.; Xing, S. X.; Chen, T.; Chen, G.; Huang, X.; Zhang, H.; Chen, H. Y. Fabrication of Polymer Nanocavities with Tailored Openings. *ACS Nano* **2009**, *3*, 3469–3474.
45. Fava, D.; Winnik, M. A.; Kumacheva, E. Photothermally-Triggered Self-Assembly of Gold Nanorods. *Chem. Commun.* **2009**, 2571–2573.
46. Yang, M. X.; Chen, G.; Zhao, Y. F.; Silber, G.; Wang, Y.; Xing, S. X.; Han, Y.; Chen, H. Y. Mechanistic Investigation into the Spontaneous Linear Assembly of Gold Nanospheres. *Phys. Chem. Chem. Phys.* **2010**, *12*, 11850–11860.
47. Chan, Y. T.; Li, S. N.; Moorefield, C. N.; Wang, P. S.; Shreiner, C. D.; Newkome, G. R. Self-Assembly, Disassembly, and Reassembly of Gold Nanorods Mediated by Bis-(terpyridine)-Metal Connectivity. *Chem.—Eur. J.* **2010**, *16*, 4164–4168.
48. Li, M.; Johnson, S.; Guo, H. T.; Dujardin, E.; Mann, S. A Generalized Mechanism for Ligand-Induced Dipolar Assembly of Plasmonic Gold Nanoparticle Chain Networks. *Adv. Funct. Mater.* **2011**, *21*, 851–859.
49. Shen, X.; Chen, L.; Li, D.; Zhu, L.; Wang, H.; Liu, C.; Wang, Y.; Xiong, Q.; Chen, H. Assembly of Colloidal Nanoparticles Directed by the Microstructures of Polycrystalline Ice. *ACS Nano* **2011**, *5*, 8426–8433.
50. Lukach, A.; Liu, K.; Therien-Aubin, H.; Kumacheva, E. Controlling the Degree of Polymerization, Bond Lengths, and Bond Angles of Plasmonic Polymers. *J. Am. Chem. Soc.* **2012**, *134*, 18853–18859.
51. Xia, H.; Su, G.; Wang, D. Size-Dependent Electrostatic Chain Growth of pH-Sensitive Hairy Nanoparticles. *Angew. Chem., Int. Ed.* **2013**, *52*, 3726–3730.
52. Zhao, Y.; Xu, L. G.; Liz-Marzan, L. M.; Kuang, H.; Ma, W.; Asenjo-Garcia, A.; de Abajo, F. J. G.; Kotov, N. A.; Wang, L. B.; Xu, C. L. Alternating Plasmonic Nanoparticle Heterochains Made by Polymerase Chain Reaction and Their Optical Properties. *J. Phys. Chem. Lett.* **2013**, *4*, 641–647.
53. Choueiri, R. M.; Klinkova, A.; Thérien-Aubin, H.; Rubinstein, M.; Kumacheva, E. Structural Transitions in Nanoparticle Assemblies Governed by Competing Nanoscale Forces. *J. Am. Chem. Soc.* **2013**, *135*, 10262–10265.
54. Liu, K.; Zhao, N.; Kumacheva, E. Self-Assembly of Inorganic Nanorods. *Chem. Soc. Rev.* **2011**, *40*, 656–671.
55. Kuang, H.; Ma, W.; Xu, L. G.; Wang, L. B.; Xu, C. L. Nanoscale Superstructures Assembled by Polymerase Chain Reaction (PCR): Programmable Construction, Structural Diversity, and Emerging Applications. *Acc. Chem. Res.* **2013**, *46*, 2341–2354.

56. Liu, K.; Lukach, A.; Sugikawa, K.; Chung, S.; Vickery, J.; Therien-Aubin, H.; Yang, B.; Rubinstein, M.; Kumacheva, E. Copolymerization of Metal Nanoparticles: A Route to Colloidal Plasmonic Copolymers. *Angew. Chem., Int. Ed.* **2014**, 10.1002/anie.201309718.
57. Thomas, J. R. Preparation and Magnetic Properties of Colloidal Cobalt Particles. *J. Appl. Phys.* **1966**, *37*, 2914–2915.
58. Puntes, V. F.; Krishnan, K. M.; Alivisatos, A. P. Colloidal Nanocrystal Shape and Size Control: The Case of Cobalt. *Science* **2001**, *291*, 2115–2117.
59. Puntes, V. F.; Zanchet, D.; Erdonmez, C. K.; Alivisatos, A. P. Synthesis of hcp-Co Nanodisks. *J. Am. Chem. Soc.* **2002**, *124*, 12874–12880.
60. Yin, Y.; Rioux, R. M.; Erdonmez, C. K.; Hughes, S.; Somorjai, G. A.; Alivisatos, A. P. Formation of Hollow Nanocrystals Through the Nanoscale Kirkendall Effect. *Science* **2004**, *304*, 711–714.
61. Huber, D. L. Synthesis, Properties, and Applications of Iron Nanoparticles. *Small* **2005**, *1*, 482–501.
62. Gao, J.; Zhang, B.; Zhang, X.; Xu, B. Magnetic-Dipolar-Interaction-Induced Self-Assembly Affords Wires of Hollow Nanocrystals of Cobalt Selenide. *Angew. Chem., Int. Ed.* **2006**, *45*, 1220–1223.
63. Korth, B. D.; Keng, P.; Shim, I.; Bowles, S. E.; Tang, C.; Kowalewski, T.; Nebesny, K. W.; Pyun, J. Polymer-Coated Ferromagnetic Colloids from Well-Defined Macromolecular Surfactants and Assembly into Nanoparticle Chains. *J. Am. Chem. Soc.* **2006**, *128*, 6562–6563.
64. Pyun, J. Nanocomposite Materials from Functional Polymers and Magnetic Colloids. *Polym. Rev.* **2007**, *47*, 231–263.
65. Keng, P. Y.; Shim, I.; Korth, B. D.; Douglas, J. F.; Pyun, J. Synthesis and Self-Assembly of Polymer-Coated Ferromagnetic Nanoparticles. *ACS Nano* **2007**, *1*, 279–292.
66. Benkoski, J. J.; Bowles, S. E.; Korth, B. D.; Jones, R. L.; Douglas, J. F.; Karim, A.; Pyun, J. Field Induced Formation of Mesoscopic Polymer Chains from Functional Ferromagnetic Colloids. *J. Am. Chem. Soc.* **2007**, *129*, 6291–6297.
67. Benkoski, J. J.; Bowles, S. E.; Jones, R. L.; Douglas, J. F.; Pyun, J.; Karim, A. Self-Assembly of Polymer-Coated Ferromagnetic Nanoparticles into Mesoscopic Polymer Chains. *J. Polym. Sci., Part B: Polym. Phys.* **2008**, *46*, 2267–2277.
68. Keng, P. Y.; Kim, B. Y.; Shim, I.-B.; Sahoo, R.; Veneman, P. E.; Armstrong, N. R.; Yoo, H.; Pemberton, J. E.; Bull, M. M.; Griebel, J. J.; et al. Colloidal Polymerization of Polymer-Coated Ferromagnetic Nanoparticles into Cobalt Oxide Nanowires. *ACS Nano* **2009**, *3*, 3143–3157.
69. Bull, M. M.; Chung, W. J.; Anderson, S. R.; Kim, S.-j.; Shim, I.-B.; Paik, H.-j.; Pyun, J. Synthesis of Ferromagnetic Polymer Coated Nanoparticles on Multi-Gram Scale with Tunable Particle Size. *J. Mater. Chem.* **2010**, *20*, 6023–6025.
70. Railsback, J. G.; Johnston-Peck, A. C.; Wang, J.; Tracy, J. B. Size-Dependent Nanoscale Kirkendall Effect During the Oxidation of Nickel Nanoparticles. *ACS Nano* **2010**, *4*, 1913–1920.
71. Kim, B. Y.; Shim, I.-B.; Araci, Z. O.; Saavedra, S. S.; Monti, O. L. A.; Armstrong, N. R.; Sahoo, R.; Srivastava, D. N.; Pyun, J. Synthesis and Colloidal Polymerization of Ferromagnetic Au-Co Nanoparticles into Au-Co3O4 Nanowires. *J. Am. Chem. Soc.* **2010**, *132*, 3234–3235.
72. Kim, B. Y.; Shim, I.-B.; Monti, O. L. A.; Pyun, J. Magnetic Self-Assembly of Gold Nanoparticle Chains using Dipolar Core-Shell Colloids. *Chem. Commun.* **2011**, *47*, 890–892.
73. Keng, P. Y.; Bull, M. M.; Shim, I.-B.; Nebesny, K. G.; Armstrong, N. R.; Sung, Y.; Char, K.; Pyun, J. Colloidal Polymerization of Polymer-Coated Ferromagnetic Cobalt Nanoparticles into Pt-Co_3O_4 Nanowires. *Chem. Mater.* **2011**, *23*, 1120–1129.
74. Kim, B. Y.; Yu, S.-H.; Kim, H. S.; Lee, D.-C.; Shim, I.-B.; Derosa, S. E.; Sung, Y.-E.; Pyun, J. Morphological Conversion of Dipolar Core−Shell Au−Co Nanoparticles into Beaded Au−Co_3O_4 Nanowires. *J. Mater. Chem.* **2011**, *21*, 14163–14166.
75. Khalil, K. S.; Sagastegui, A.; Li, Y.; Tahir, M. A.; Socolar, J. E. S.; Wiley, B. J.; Yellen, B. B. Binary Colloidal Structures Assembled Through Ising Interactions. *Nat. Commun.* **2012**, *3*, 1798.
76. Hill, L.; Pyun, J. Colloidal Polymers *via* Dipolar Assembly of Magnetic Nanoparticle Monomers. *ACS Appl. Mater. Interfaces* **2014**, 10.1021/am405786u.
77. Fermigier, M.; Gast, A. P. Structure Evolution in a Paramagnetic Latex Suspension. *J. Colloid Interface Sci.* **1992**, *154*, 522–539.
78. Furst, E. M.; Gast, A. P. Micromechanics of Dipolar Chains Using Optical Tweezers. *Phys. Rev. Lett.* **1999**, *82*, 4130–4133.
79. Dreyfus, R.; Baudry, J.; Roper, M. L.; Fermigier, M.; Stone, H. A.; Bibette, J. Microscopic Artificial Swimmers. *Nature* **2005**, *437*, 862–865.
80. Zerrouki, D.; Baudry, J.; Pine, D.; Chaikin, P.; Bibette, J. Chiral Colloidal Clusters. *Nature* **2008**, *455*, 380–382.
81. Sacanna, S.; Rossi, L.; Pine, D. J. Magnetic Click Colloidal Assembly. *J. Am. Chem. Soc.* **2012**, *134*, 6112–6115.
82. Odian, G., *Principles of Polymerization*, 4th ed.; Wiley: New York, 2004.
83. Wang, H.; Chen, L.; Shen, X.; Zhu, L.; He, J.; Chen, H. Unconventional Chain-Growth Mode in the Assembly of Colloidal Gold Nanoparticles. *Angew. Chem., Int. Ed.* **2012**, *51*, 8021–8025.
84. Shibu Joseph, S. T.; Ipe, B. I.; Pramod, P.; Thomas, K. G. Gold Nanorods to Nanochains: Mechanistic Investigations on Their Longitudinal Assembly Using α,ω-Alkanedithiols and Interplasmon Coupling. *J. Phys. Chem. B* **2005**, *110*, 150–157.
85. Liu, K.; Nie, Z.; Zhao, N.; Li, W.; Rubinstein, M.; Kumacheva, E. Step-Growth Polymerization of Inorganic Nanoparticles. *Science* **2010**, *329*, 197–200.
86. Liu, K.; Resetco, C.; Kumacheva, E. Salt-Mediated Kinetics of the Self-Assembly of Gold Nanorods End-Tethered with Polymer Ligands. *Nanoscale* **2012**, *4*, 6574–6580.
87. Klinkova, A.; Thérien-Aubin, H.; Choueiri, R. M.; Rubinstein, M.; Kumacheva, E. Colloidal Analogs of Molecular Chain Stoppers. *Proc. Natl. Acad. Sci. U.S.A.* **2013**, *110*, 18775–18779.
88. Buonsanti, R.; Grillo, V.; Carlino, E.; Giannini, C.; Curri, M. L.; Innocenti, C.; Sangregorio, C.; Achterhold, K.; Parak, F. G.; Agostiano, A.; et al. Seeded Growth of Asymmetric Binary Nanocrystals Made of a Semiconductor TiO_2 Rodlike Section and a Magnetic Gamma-Fe_2O_3 Spherical Domain. *J. Am. Chem. Soc.* **2006**, *128*, 16953–16970.
89. Casavola, M.; Grillo, V.; Carlino, E.; Giannini, C.; Gozzo, F.; Fernandez Pinel, E.; Garcia, M. A.; Manna, L.; Cingolani, R.; Cozzoli, P. D. Topologically Controlled Growth of Magnetic-Metal-Functionalized Semiconductor Oxide Nanorods. *Nano Lett.* **2007**, *7*, 1386–1395.
90. Zanella, M.; Falqui, A.; Kudera, S.; Manna, L.; Casula, M. F.; Parak, W. J. Growth of Colloidal Nanoparticles of Group II−VI and IV−VI Semiconductors on top of Magnetic Iron−Platinum Nanocrystals. *J. Mater. Chem.* **2008**, *18*, 4311.
91. Buonsanti, R.; Snoeck, E.; Giannini, C.; Gozzo, F.; Garcia-Hernandez, M.; Garcia, M. A.; Cingolani, R.; Cozzoli, P. D. Colloidal Semiconductor/Magnetic Heterostructures Based on Iron-Oxide-Functionalized Brookite TiO_2 nanorods. *Phys. Chem. Chem. Phys.* **2009**, *11*, 3680–3691.
92. Casavola, M.; Falqui, A.; Garcia, M. A.; Garcia-Hernandez, M.; Giannini, C.; Cingolani, R.; Cozzoli, P. D. Exchange-Coupled Bimagnetic Cobalt/Iron Oxide Branched Nanocrystal Heterostructures. *Nano Lett.* **2009**, *9*, 366–376.
93. Deka, S.; Falqui, A.; Bertoni, G.; Sangregorio, C.; Poneti, G.; Morello, G.; De Giorgi, M.; Giannini, C.; Cingolani, R.; Manna, L.; et al. Fluorescent Asymmetrically Cobalt-Tipped CdSe@CdS Core@Shell Nanorod Heterostructures Exhibiting Room-Temperature Ferromagnetic Behavior. *J. Am. Chem. Soc.* **2009**, *131*, 12817–12828.

94. Buonsanti, R.; Grillo, V.; Carlino, E.; Giannini, C.; Gozzo, F.; Garcia-Hernandez, M.; Garcia, M. A.; Cingolani, R.; Cozzoli, P. D. Architectural Control of Seeded-Grown Magnetic-Semicondutor Iron Oxide-TiO_2 Nanorod Heterostructures: The Role of Seeds in Topology Selection. *J. Am. Chem. Soc.* **2010**, *132*, 2437–2464.
95. Maynadie, J.; Salant, A.; Falqui, A.; Respaud, M.; Shaviv, E.; Banin, U.; Soulantica, K.; Chaudret, B. Cobalt Growth on the Tips of CdSe Nanorods. *Angew. Chem.* **2009**, *48*, 1814–1817.
96. Sheiko, S. S.; Sumerlin, B. S.; Matyjaszewski, K. Cylindrical Molecular Brushes: Synthesis, Characterization, and Properties. *Prog. Polym. Sci.* **2008**, *33*, 759–785.
97. Hill, L. J.; Bull, M. M.; Sung, Y.; Simmonds, A. G.; Dirlam, P. T.; Richey, N. E.; DeRosa, S. E.; Shim, I.-B.; Guin, D.; Costanzo, P. J.; et al. Directing the Deposition of Ferromagnetic Cobalt onto Pt-Tipped CdSe@CdS Nanorods: Synthetic and Mechanistic Insights. *ACS Nano* **2012**, *6*, 8632–8645.
98. Carbone, L.; Nobile, C.; De Giorgi, M.; Sala, F. D.; Morello, G.; Pompa, P.; Hytch, M.; Snoeck, E.; Fiore, A.; Franchini, I. R.; et al. Synthesis and Micrometer-Scale Assembly of Colloidal CdSe/CdS Nanorods Prepared by a Seeded Growth Approach. *Nano Lett.* **2007**, *7*, 2942–2950.
99. Habas, S. E.; Yang, P. D.; Mokari, T. Selective Growth of Metal and Binary Metal Tips on CdS Nanorods. *J. Am. Chem. Soc.* **2008**, *130*, 3294–3295.
100. Xu, J.; Wang, H.; Liu, C.; Yang, Y.; Chen, T.; Wang, Y.; Wang, F.; Liu, X.; Xing, B.; Chen, H. Mechanical Nanosprings: Induced Coiling and Uncoiling of Ultrathin Au Nanowires. *J. Am. Chem. Soc.* **2010**, *132*, 11920–11922.
101. Chen, L.; Wang, H.; Xu, J.; Shen, X.; Yao, L.; Zhu, L.; Zeng, Z.; Zhang, H.; Chen, H. Controlling Reversible Elastic Deformation of Carbon Nanotube Rings. *J. Am. Chem. Soc.* **2011**, *133*, 9654–9657.
102. Chen, L.; Yu, S.; Wang, H.; Xu, J.; Liu, C.; Chong, W. H.; Chen, H. General Methodology of Using Oil-in-Water and Water-in-Oil Emulsions for Coiling Nanofilaments. *J. Am. Chem. Soc.* **2013**, *135*, 835–843.
103. Singh, H.; Laibinis, P. E.; Hatton, T. A. Rigid, Superparamagnetic Chains of Permanently Linked Beads Coated with Magnetic Nanoparticles. Synthesis and Rotational Dynamics under Applied Magnetic Fields. *Langmuir* **2005**, *21*, 11500–11509.
104. Neugebauer, D.; Sumerlin, B. S.; Matyjaszewski, K.; Goodhart, B.; Sheiko, S. S. How Dense are Cylindrical Brushes Grafted from a Multifunctional Macroinitiator? *Polymer* **2004**, *45*, 8173–8179.
105. Van Workum, K.; Douglas, J. F. Equilibrium Polymerization in the Stockmayer Fluid as a Model of Supermolecular Self-Organization. *Phys. Rev. E* **2005**, *71*, 031502.
106. Van Workum, K.; Douglas, J. F. Symmetry, Equivalence, and Molecular Self-Assembly. *Phys. Rev. E* **2006**, *73*, 031502.
107. Tlusty, T.; Safran, S. A. Defect-Induced Phase Separation in Dipolar Fluids. *Science* **2000**, *290*, 1328–1331.
108. Kindt, J. T. Simulation and Theory of Self-Assembled Networks: Ends, Junctions, and Loops. *J. Phys. Chem. B* **2002**, *106*, 8223–8232.
109. Lavender, H. B.; Iyer, K. A.; Singer, S. J. Global Orientational Order in Model Polar Clusters. *J. Chem. Phys.* **1994**, *101*, 7856–7867.
110. Xu, C.; Xu, K.; Gu, H.; Zhong, X.; Guo, Z.; Zheng, R.; Zhang, X.; Xu, B. Nitrilotriacetic Acid-Modified Magnetic Nanoparticles as a General Agent to Bind Histidine-Tagged Proteins. *J. Am. Chem. Soc.* **2004**, *126*, 3392–3393.
111. Gu, H.; Xu, K.; Xu, C.; Xu, B. Biofunctional Magnetic Nanoparticles for Protein Separation and Pathogen Detection. *Chem. Commun.* **2006**, 941–949.
112. Samia, A. C. S.; Hyzer, K.; Schlueter, J. A.; Qin, C.-J.; Jiang, J. S.; Bader, S. D.; Lin, X.-M. Ligand Effect on the Growth and the Digestion of Co Nanocrystals. *J. Am. Chem. Soc.* **2005**, *127*, 4126–4127.